

Stabilization of BEC droplet in free space by feedback control of interatomic interaction

Hiroki Saito¹ and Masahito Ueda^{2,3}

¹*Department of Applied Physics and Chemistry, The University of Electro-Communications, Tokyo 182-8585, Japan*

²*Department of Physics, Tokyo Institute of Technology, Tokyo 152-8551, Japan*

³*ERATO, Japan Science and Technology Corporation (JST), Saitama 332-0012, Japan*

(Dated: May 1, 2019)

A self-trapped Bose-Einstein condensate in three-dimensional free space is shown to be stabilized by feedback control of the interatomic interaction through nondestructive measurement of the condensate's peak column density. The stability is found to be robust against poor resolution and experimental errors in the measurement.

PACS numbers: 03.75.Lm, 03.75.Kk, 02.30.Yy, 05.45.Yv

I. INTRODUCTION

Matter-wave bright solitons of a Bose-Einstein condensate (BEC) in a quasi-one dimensional (1D) trapping potential have been realized by the ENS group [1] and the Rice group [2]. The stability of this self-trapped state is achieved by the balance between the attractive interatomic interaction and the quantum kinetic pressure. In 1D, the bright soliton is stable and robust against noise. In 2D and 3D, however, the balance between the attractive interaction and the kinetic pressure is precarious, and infinitesimal deviations from the stationary state cause a collapse or expansion of the system. While self-trapped liquids, such as a raindrop, are quite common, a self-trapped gas is a novel state of matter. Such a stable self-trapped state in a gaseous BEC in 2D or 3D, if it can be realized, might be referred to as a matter-wave droplet or simply a BEC droplet.

A scheme proposed in Refs. [3, 4] to stabilize a BEC droplet is to oscillate the interatomic interaction rapidly using Feshbach resonance [5, 6]. The rapid oscillation of the interaction produces an effective potential that prevents the condensate from collapsing. This phenomenon is similar to the stabilization of an inverted pendulum by an oscillating pivot [7]. Several researchers have demonstrated the stabilization of a BEC droplet in 2D with oscillating interactions by numerically solving the Gross-Pitaevskii (GP) equation [3, 4, 8, 9]. Montesinos *et al.* [10] have shown that this stabilization in 2D is also possible for a multicomponent BEC. Matuszewski *et al.* [11] have predicted 3D breather solitons confined in a 1D lattice. However, in 3D free space, it appears that an oscillating interaction alone cannot stabilize a BEC droplet due to dynamical instabilities [4, 8]. By taking into account the effect of energy dissipation, which always exists in realistic situations, we have shown that a BEC droplet with oscillating interactions can be stabilized in 3D [12].

In the present paper, we show that a BEC droplet in 3D free space can be stabilized by feedback control of the interaction through nondestructive measurement of the condensate's peak column density. Real-time moni-

toring of the density profile of a condensate is possible by using a nondestructive in-situ imaging method [13]. The collapse or expansion of the condensate can be prevented by a decrease or increase, respectively, in the strength of the attractive interaction if the peak density of the condensate increases above or decreases below a prescribed value. Thus, the shape of the BEC droplet can be maintained without collapse or expansion by negative feedback from the result of the real-time measurement. We will also examine the effect of experimental imperfections in the real-time measurement, such as spatial and time resolutions and experimental errors, and show that the stabilized BEC droplet is robust against these imperfections.

This paper is organized as follows. Section II discusses the stationary solutions of the GP equations in 1D, 2D, and 3D free space. Section III numerically investigates the dynamics of the condensate under feedback control, and shows that a BEC droplet in 3D can be stabilized for a wide range of parameters. Section IV presents variational analysis using a Gaussian trial function. Section V studies the stability against measurement errors and finite measurement resolution, and shows that a BEC droplet is robust against these experimental imperfections. Finally, Sec. VI concludes this paper.

II. STATIONARY SOLUTIONS OF THE GROSS-PITAEVSKII EQUATION IN FREE SPACE

We first consider a stationary state of a BEC with an attractive interaction in free space. The dynamics of the BEC are described by the GP equation,

$$i\hbar\frac{\partial\psi}{\partial t} = -\frac{\hbar^2}{2m}\nabla^2\psi + V\psi + \frac{4\pi\hbar^2 a}{m}|\psi|^2\psi, \quad (1)$$

where m is the mass of an atom, V is the external potential, and a is the s -wave scattering length. The wave function is normalized with $\int|\psi|^2 d\mathbf{r} = N$, with N being the number of atoms.

When the external potential is given by $V = m\omega_{1d}^2(x^2 + y^2)/2$ and $\hbar\omega_{1d}$ is much larger than the other

characteristic energies, the degrees of freedom of the BEC in the x and y directions are frozen and the system behaves as an effective 1D system. Writing the wave function as

$$\psi(\mathbf{r}) = \sqrt{\frac{m\omega_{1d}}{\pi\hbar}} e^{-\frac{m\omega_{1d}}{2\hbar}(x^2+y^2)-i\omega_{1d}t} \psi_z(z), \quad (2)$$

and integrating Eq. (1) over x and y , we obtain an effective 1D equation:

$$i\hbar \frac{\partial \psi_z}{\partial t} = -\frac{\hbar^2}{2m} \frac{\partial^2 \psi_z}{\partial z^2} + g_{1d} |\psi_z|^2 \psi_z, \quad (3)$$

where $g_{1d} = 2\hbar\omega_{1d}a$. If $a < 0$, this equation has a well-known soliton solution [14]:

$$\psi_z = e^{-i\mu t/\hbar} \sqrt{\frac{\eta N}{2}} \operatorname{sech} \eta(z - z_0), \quad (4)$$

where $\mu = -m\omega_{1d}^2 a^2 N^2/2$, $\eta = m\omega_{1d}|a|N/\hbar$, and z_0 is the position of the peak. This is the ground state solution, and it has no dynamical instabilities. Thus an attractive BEC is stable in 1D.

When $V = m\omega_{2d}^2 z^2/2$ and $\hbar\omega_{2d}$ is much larger than the other characteristic energies, the system behaves as an effective 2D system. Substituting the wave function

$$\psi(\mathbf{r}) = \left(\frac{m\omega_{2d}}{\pi\hbar}\right)^{1/4} e^{-\frac{m\omega_{2d}}{2\hbar}z^2 - i\frac{\omega_{2d}}{2}t} \psi_{xy}(x, y) \quad (5)$$

into Eq. (1), and integrating the result over z , we obtain an effective 2D equation:

$$i\hbar \frac{\partial \psi_{xy}}{\partial t} = -\frac{\hbar^2}{2m} \left(\frac{\partial^2}{\partial x^2} + \frac{\partial^2}{\partial y^2} \right) \psi_{xy} + g_{2d} |\psi_{xy}|^2 \psi_{xy}, \quad (6)$$

where $g_{2d} = (8\pi\hbar^3 a^2 \omega_{2d}/m)^{1/2}$. At the critical strength of the interaction

$$g_{2d}^{\text{cr}} \simeq -1.862 \frac{\pi\hbar^2}{mN}, \quad (7)$$

Eq. (6) has a stationary self-trapped solution, which is known as the Townes soliton [15]. If the peak of the Townes soliton is located at the origin $\mathbf{r} = 0$, the wave function is axisymmetric and the density $|\psi|^2$ monotonically decreases to zero for $r \rightarrow \infty$. The Townes soliton also has a scaling property; if $\psi_{xy}(x, y)$ is a stationary solution of Eq. (6), the scaled wave function $\alpha\psi_{xy}(\alpha x, \alpha y)$ with an arbitrary scaling parameter α is also a stationary solution of Eq. (6). However, the Townes soliton is dynamically unstable in the sense that an infinitesimal deviation from the stationary solution grows exponentially in time, and therefore the Townes soliton eventually collapses or expands.

When $V = 0$, i.e., in 3D free space, Eq. (1) with $a < 0$ has a stationary self-trapped solution that is dynamically unstable like the Townes soliton. The density of this stationary solution has spherical symmetry and monotonically decreases to zero for $r \rightarrow \infty$ [16]. The striking difference between this 3D stationary state and the Townes

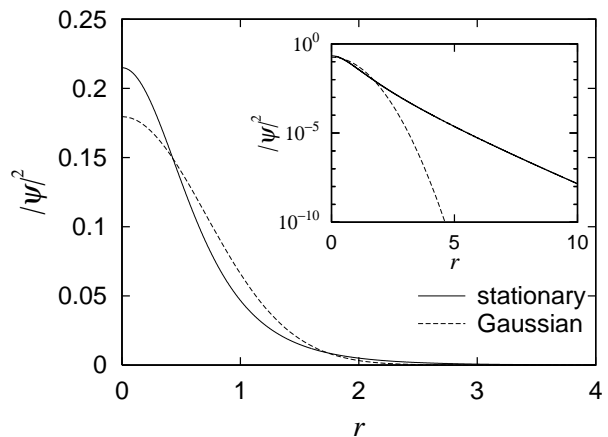


FIG. 1: Stationary unstable solution of Eq. (8) (solid curve) for $g = -(2\pi)^{3/2}$. The Gaussian function $e^{-r^2}/\pi^{3/2}$ is superimposed as a dashed curve for comparison. See Sec. IV for the choice of parameters. The inset shows the same functions on a logarithmic scale to show the difference in the large- r behavior.

soliton is in their scaling properties. Normalizing the length, time, and wave function in units of ℓ , $m\ell^2/\hbar$, and $(N/\ell^3)^{1/2}$, respectively, where ℓ is an arbitrary length scale, Eq. (1) reduces to

$$i \frac{\partial \psi}{\partial t} = -\frac{\nabla^2}{2} \psi + g |\psi|^2 \psi, \quad (8)$$

where $g = 4\pi Na/\ell$. Therefore, if $\psi(\mathbf{r}, t)$ is a solution of the GP equation with scattering length a , the scaled wave function $\alpha^{3/2}\psi(\alpha\mathbf{r}, \alpha^2 t)$ also satisfies the GP equation with scattering length a/α . This indicates that there always exists an unstable stationary solution for any $g < 0$, and the solutions for different g 's are related by the scaling transformation. In contrast, in 2D, the Townes soliton exists only for a particular value of $g_{2d} = g_{2d}^{\text{cr}}$ (see Eq. (7)) for an arbitrary scaling parameter α .

In Fig. 1, we plot the density profile of the unstable stationary state in 3D for $g = -(2\pi)^{3/2}$, which is numerically obtained by the Newton–Raphson method [17]. The inset of Fig. 1 shows the logarithmic plot of the large- r behavior. We find that the tail of the unstable stationary state (solid curve) is longer than that of the Gaussian wave function $e^{-r^2}/\pi^{3/2}$ (dashed curve). Generally, in d dimensions the unstable stationary wave function has an asymptotic form $r^{(1-d)/2} e^{-cr}$ with constant c for $r \rightarrow \infty$ [16]. The dependence of the tail on r in the inset of Fig. 1 is consistent with this functional form with $d = 3$ and $c \simeq 1.3$.

III. FEEDBACK CONTROL OF A BEC DROPLET

The 3D stationary solution of Eq. (8) is dynamically unstable against collapse and expansion. The aim of

the present paper is to show that we can stabilize it by controlling the scattering length a . When the system is about to collapse, we can increase a to prevent the collapse. Similarly, a decrease in a can prevent expansion. Thus, by measuring the density profile of the condensate in a nondestructive manner, we can achieve feedback control of a to stabilize a BEC droplet.

An observable quantity in nondestructive phase-contrast imaging [13] is the column density of the condensate, given by

$$d_{\text{col}}(x, y, t) = \int dz |\psi(\mathbf{r}, t)|^2, \quad (9)$$

where the line of sight is assumed to be in the z direction. We use the peak value of the column density,

$$D \equiv d_{\text{col}}(0, 0, t), \quad (10)$$

for the feedback control.

Let D_0 be the target value of the stabilized column density. The feedback loop should operate on the strength of the interaction g in such a manner that any deviation $\tilde{D} \equiv D - D_0$ from the target value D_0 will be suppressed. We assume that the time derivative of g depends on \tilde{D} up to the second derivative with respect to time:

$$\dot{g} = A(D - D_0) + B\dot{\tilde{D}} + C\ddot{\tilde{D}}, \quad (11)$$

where A , B , and C are dimensionless constants. Recovering the dimensions of D and t by multiplying by N/ℓ^2 and $m\ell^2/\hbar$, respectively, where ℓ is an arbitrary unit of length, we can write Eq. (11) as

$$\dot{a} = \frac{\ell\hbar}{4\pi N^2 m} A(D - D_0) + \frac{\ell^3}{4\pi N^2} B\dot{\tilde{D}} + \frac{m\ell^5}{4\pi N^2 \hbar} C\ddot{\tilde{D}}. \quad (12)$$

In experiments, a time sequence of phase-contrast images is taken by a CCD camera at a certain frame rate (e.g., 20 kHz in Ref. [18]). Therefore, the measurement of D is performed at discrete times and the time derivatives in Eq. (11) are approximately obtained by

$$\dot{D}(t) \simeq \frac{1}{\Delta t} [D(t) - D(t - \Delta t)], \quad (13a)$$

$$\ddot{D}(t) \simeq \frac{1}{\Delta t^2} [D(t) - 2D(t - \Delta t) + D(t - 2\Delta t)], \quad (13b)$$

where Δt is the interval between measurements. Accordingly, g is also changed stepwise as

$$g(t) = g(t - \Delta t) + \Delta t \left\{ A[D(t) - D_0] + B\dot{D}(t) + C\ddot{D}(t) \right\}, \quad (14)$$

where Eqs. (13a) and (13b) are used for $\dot{D}(t)$ and $\ddot{D}(t)$. The interval Δt must be made much smaller than the characteristic time scale of the dynamics. The Δt dependence of the stability is discussed in Sec. V.

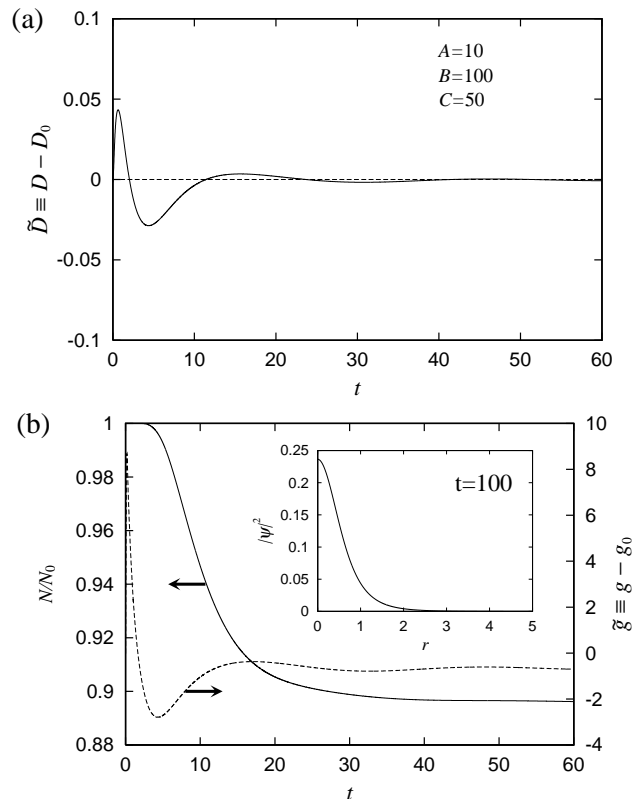


FIG. 2: Time evolution of (a) the deviation $\tilde{D} \equiv D - D_0$ of the peak column density (see Eqs. (9) and (10)) and (b) the fraction of remaining atoms N/N_0 (solid curve) and the strength of the interaction $\tilde{g} = g - g_0$ (dashed curve), for $A = 10$, $B = 100$, $C = 50$, $\Delta t = 0.01$, $D_0 = 1/\pi$, and $g_0 = -(2\pi)^{3/2}$. The initial state is the Gaussian wave function $\psi = e^{-r^2/2}/\pi^{3/4}$, and the value of \tilde{g} starts from 0 (not visible in the present resolution). The inset in (b) shows the converged density profile $|\psi|^2$ at $t = 100$.

We assume that the initial state is the noninteracting ground state in an isotropic harmonic potential $V = m\omega^2 \mathbf{r}^2/2$. Henceforth, we take the units of length and time to be $\ell = [\hbar/(m\omega)]^{1/2}$ and ω^{-1} , respectively. The initial state is then described by the Gaussian wave function $\psi = e^{-r^2/2}/\pi^{3/4}$. At $t = 0$, the trapping potential is suddenly switched off and the strength of the interaction is set to be $g = -(2\pi)^{3/2}$. The strength of the interaction g evolves in time according to Eq. (14), where the value of D_0 is chosen to be the peak column density of the initial wave function, $D_0 = \int dz |\psi(x = 0, y = 0, z, t = 0)|^2 = 1/\pi$. The wave function evolves in time according to Eq. (8), which is numerically solved by the Crank–Nicolson method. We neglect the effect of gravity by assuming that it is canceled using, e.g., a technique of magnetic levitation [19].

Figure 2 (a) shows the time evolution of D for $A = 10$, $B = 100$, $C = 50$, and $\Delta t = 0.01$. The value of D deviates significantly from D_0 only for $t \lesssim 20$, and quickly converges to D_0 thereafter. This indicates that

the feedback control of the interaction successfully works to stabilize a BEC droplet in 3D. The inset in Fig. 2 (b) shows the density profile of the condensate at $t = 100$. This converged density profile is found to be related to the stationary solution of Eq. (8) by appropriate scaling. The feedback control can thus transform a Gaussian wave function into a stationary solution of Eq. (8). During this transformation, a certain fraction of atoms are lost from the condensate. The solid curve in Fig. 2 (b) shows the fraction of atoms remaining within the radius $r = 10$ around the center of the condensate,

$$\frac{N}{N_0} = \int_0^{10} dr 4\pi r^2 |\psi|^2. \quad (15)$$

We find that roughly 10% of atoms are scattered away from the condensate without returning to the center due to the lack of a trapping potential.

Figure 3 shows the dependence of the dynamics on the feedback parameters. Figure 3 (a) shows that the parameter A controls the amplitude of the density oscillation. The oscillation frequency increases with an increase in A , and for large A the system becomes unstable against the growth in the amplitude of the density oscillations. This is because the term of A in Eq. (11) plays a role of pulling the value of D back to D_0 . If A is too large, this pulling causes an overshoot, resulting in oscillations of D . Figures 3 (b) and (c) indicate that the amplitudes of the oscillations decrease with increasing B and C . The decay of the oscillations accelerates for larger B [Fig. 3 (b)], while it decelerates for larger C [Fig. 3 (c)].

Figure 4 shows a stability diagram of the feedback control with respect to the feedback parameters B and C . We take the value $A = 10$, since larger values of A cause rapid oscillations of the system, as shown in Fig. 3 (a). We find that the BEC droplet can be stabilized for $B \gtrsim 30$ and $C \gtrsim -20$.

IV. VARIATIONAL ANALYSIS

In order to understand in an analytic manner the stability of the system subject to the feedback control discussed in Sec. III, we conduct a variational analysis.

We employ the Gaussian trial function [20]

$$\psi_G = \frac{1}{\pi^{3/4} R^{3/2}} e^{-\frac{r^2}{2R^2} + i\frac{\dot{R}}{2R} r^2}, \quad (16)$$

where $R(t)$ is a variational parameter that characterizes the size of the condensate. Equation (8) is derived by the application of the variational principle to the action

$$S = \int dr dt \psi^* \left(i \frac{\partial}{\partial t} + \frac{\nabla^2}{2} - \frac{g}{2} |\psi|^2 \right) \psi. \quad (17)$$

Substituting the variational wave function (16) into Eq. (17) and minimizing the result with respect to R , we obtain the equation of motion for R as

$$\ddot{R} = -\frac{1}{R^3} - \frac{g}{(2\pi)^{3/2}} \frac{1}{R^4}. \quad (18)$$

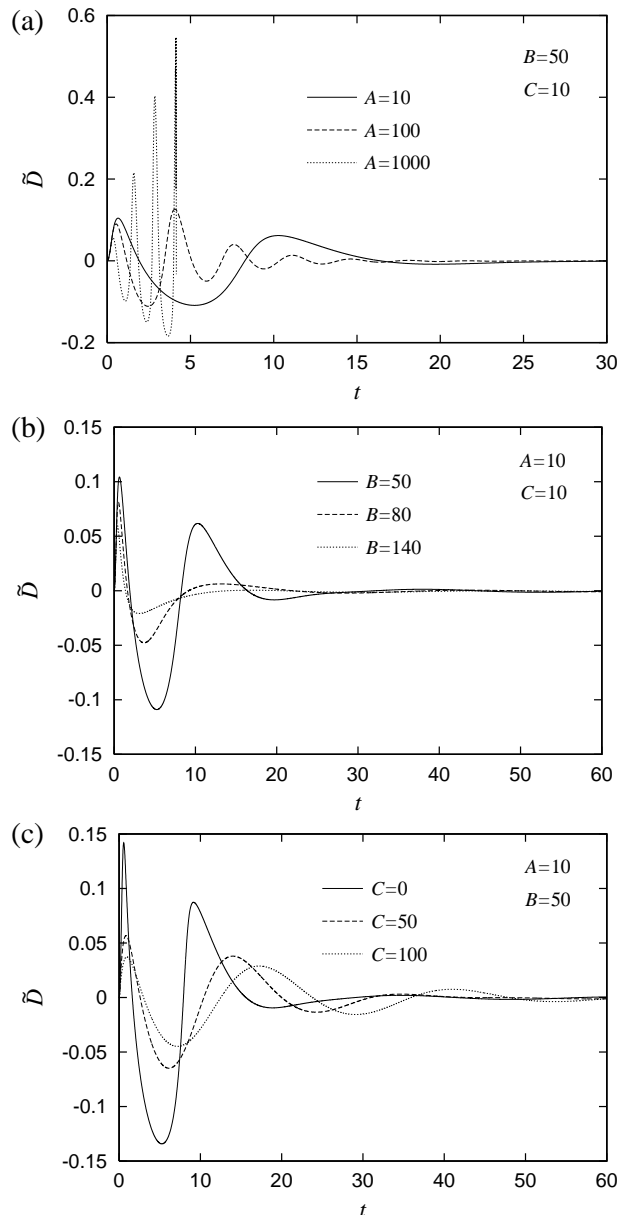


FIG. 3: Dependence of the dynamics of D on the feedback parameters A , B , and C . The other conditions are the same as in Fig. 2.

The unstable stationary solution of Eq. (18) is obtained for $R = -g/(2\pi)^{3/2}$; hence, if $g = -(2\pi)^{3/2}$, we have $R = 1$. In Fig. 1, we plot the Gaussian function (16) with $R = 1$ as a dashed curve. Comparing it with the numerically obtained stationary solution of Eq. (8) with $g = -(2\pi)^{3/2}$ (solid curve), we see that the central density is larger and the tail is longer for the stationary solution than for the Gaussian function.

Since R cannot directly be measured in experiments, we rewrite the equation of motion in terms of the central

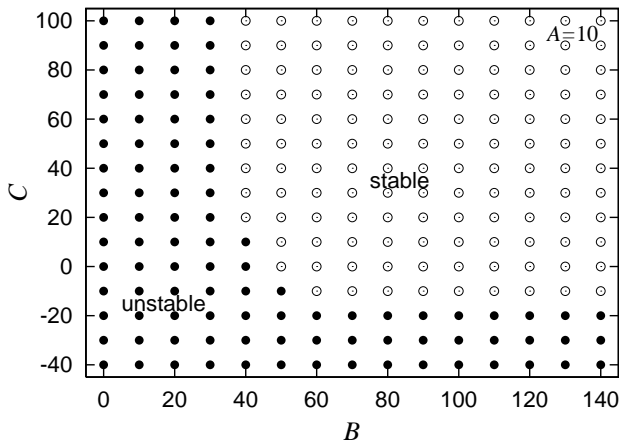


FIG. 4: Stability diagram of the BEC droplet under feedback control for $A = 10$. The other conditions are the same as in Fig. 2. The open circles show stable points and the filled circles show unstable points.

column density

$$D = 2 \int_0^\infty dr |\psi_G|^2 = \frac{1}{\pi R^2}. \quad (19)$$

We consider small deviations from $g_0 = -(2\pi)^{3/2}$ and $R_0 = 1$, and decompose D and g as $D = D_0 + \tilde{D}$ and $g = g_0 + \tilde{g}$, where $D_0 = 1/\pi$. Equation (18) can then be rewritten as

$$\ddot{\tilde{D}} = \tilde{D} - \frac{1}{\sqrt{2}\pi^{5/2}} \tilde{g}, \quad (20)$$

where we have kept only the terms linear in $|\tilde{D}|$ and $|\tilde{g}|$. From Eq. (11), we have

$$\dot{\tilde{g}} = A\tilde{D} + B\dot{\tilde{D}} + C\ddot{\tilde{D}}. \quad (21)$$

Differentiating Eq. (20) with respect to t and using Eq. (21), we obtain

$$\frac{d}{dt} \begin{pmatrix} \tilde{D} \\ \dot{\tilde{D}} \\ \ddot{\tilde{D}} \end{pmatrix} = \begin{pmatrix} 0 & 1 & 0 \\ 0 & 0 & 1 \\ -\frac{A}{\sqrt{2}\pi^{5/2}} & 1 - \frac{B}{\sqrt{2}\pi^{5/2}} & -\frac{C}{\sqrt{2}\pi^{5/2}} \end{pmatrix} \begin{pmatrix} \tilde{D} \\ \dot{\tilde{D}} \\ \ddot{\tilde{D}} \end{pmatrix}. \quad (22)$$

If the 3×3 matrix in Eq. (22) has an eigenvalue whose real part is positive, \tilde{D} diverges exponentially in time. Therefore, the condition for stability is that all the eigenvalues have negative real parts, which can be examined by using the Routh-Hurwitz criterion [21] without actually solving the eigenvalue equation. The stability condition of Eq. (22) is found to be (see Appendix A for derivation)

$$A > 0, \quad (23a)$$

$$B > \sqrt{2}\pi^{5/2}, \quad (23b)$$

$$C > 0, \quad (23c)$$

$$A < C \left(\frac{B}{\sqrt{2}\pi^{5/2}} - 1 \right). \quad (23d)$$

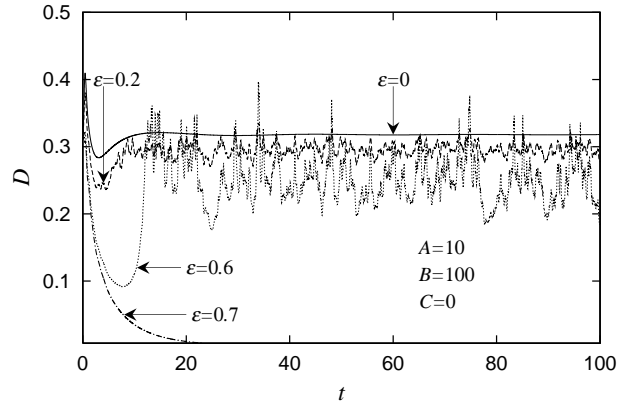


FIG. 5: Time evolution of the peak column density D with measurement errors given in Eq. (24) for $\varepsilon = 0$ (solid line), $\varepsilon = 0.2$ (dashed line), $\varepsilon = 0.6$ (dotted line), and $\varepsilon = 0.7$ (dot-dashed line). The feedback parameters are $A = 10$, $B = 100$, and $C = 0$. The other conditions are the same as in Fig. 2.

These inequalities qualitatively agree with the stability diagram in Fig. 4.

V. EFFECTS OF EXPERIMENTAL IMPERFECTIONS ON THE STABILITY OF FEEDBACK CONTROL

We have so far assumed that the peak column density D can be measured precisely. However, in real experiments, there are always imperfections in the measurement, such as errors and the finite resolution of time and space. In this section, we investigate the effects of such imperfections on the stability of our feedback control.

We first study the effects of measurement errors of D on the stability. We assume that the measured value with an error is given by

$$D_\varepsilon = D(1 + \varepsilon v_{\text{rnd}}), \quad (24)$$

where D is defined by Eq. (10), ε describes the error level, and v_{rnd} is a random variable that simulates the measurement error and is assumed to obey the normal distribution $e^{-v_{\text{rnd}}^2/2}/\sqrt{2\pi}$. Figure 5 shows some examples of the time evolution of D , in which D_ε is used in the feedback equation (11) instead of D . We find that the system is tolerant against an error level up to about 60% in every measurement, and the stability is excellent. In Fig. 5, we see that D has a tendency to decrease with an increase in ε . This phenomenon is similar to that in the case of oscillating interactions [3, 4], where the peak density is suppressed by the oscillation of the interaction. In the present case, the random fluctuations in g play the role of oscillating interactions.

We next study the effect on the stability of the spatial resolution in the measurement of D . We assume that due to the finite spatial resolution, the measured value is

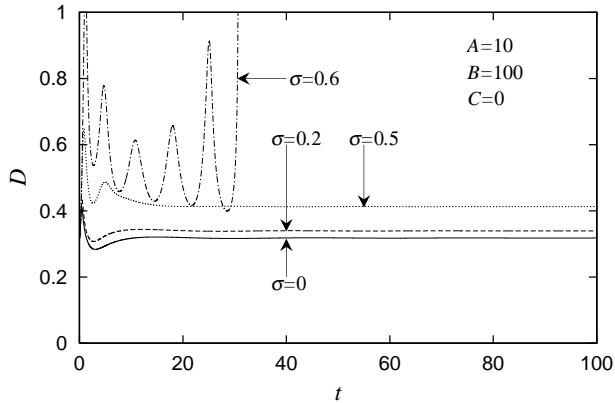


FIG. 6: Time evolution of the peak column density D with spatial resolution given in Eq. (25) for $\sigma = 0$ (solid line), $\sigma = 0.2$ (dashed line), $\sigma = 0.5$ (dotted line), and $\sigma = 0.6$ (dot-dashed line). The feedback parameters are $A = 10$, $B = 100$, and $C = 0$. The other conditions are the same as in Fig. 2.

filtered by a Gaussian function,

$$D_\sigma = \int dx dy \frac{1}{2\pi\sigma^2} e^{-\frac{x^2+y^2}{2\sigma^2}} d_{\text{col}}(x, y), \quad (25)$$

where $d_{\text{col}}(x, y)$ is given in Eq. (9) and σ characterizes the spatial resolution. Figure 6 shows the time evolution of D , in which D_σ is used in Eq. (11) instead of D . It is remarkable that the stability is very robust against low resolution. In fact, Fig. 6 shows that the acceptable resolution can be almost the size of the condensate itself.

We have assumed so far that the successive measurements are performed at an interval of $\Delta t = 0.01$. We have also examined the stability for larger Δt with $A = 10$, $B = 100$, and $C = 0$ (with the other conditions the same as in Fig. 2), and found that stability is achieved for a time interval of up to $\Delta t = 0.4$.

As an example, let us consider the case of ^{85}Rb atoms and take the units of length and time to be $3.5\mu\text{m}$ and 16 ms , which corresponds to $\omega = 10 \times 2\pi\text{ Hz}$. Then, the resolution of the phase-contrast imaging must be $\sigma \lesssim 1.7\mu\text{m}$, and the interval of the measurements must be $\Delta t \lesssim 6.4\text{ ms}$, which corresponds to a frame rate $\gtrsim 160\text{ Hz}$. If we use a larger condensate (i.e., a smaller ω), these restrictions can be relaxed.

VI. CONCLUSIONS

We have shown that a BEC droplet (self-trapped condensate) can be stabilized in 3D free space by the feedback control of the strength of the interaction between atoms. By negative feedback on the strength of the interaction through nondestructive monitoring of the peak column density of the condensate, we can prevent the condensate from collapsing and expanding. Even starting from a Gaussian wave function, we can reach the stationary state of the GP equation by feedback control.

We have considered the feedback from the peak column density D and its time derivatives \dot{D} and \ddot{D} (Eq. (11)), and have examined the stability of the system for various values of the parameters. We found that stability is obtained for a wide range of parameters, as shown in Figs. 3 and 4.

We have also investigated the stability against experimental imperfections, such as measurement errors (Fig. 5), finite spatial resolution (Fig. 6), and finite time intervals between measurements. We have found that the stability is robust against these imperfections.

In this paper, we have considered only the simplest form of negative feedback. More robust stability may be obtained and the stationary state may be reached more quickly if more sophisticated methods are used, such as the Kalman filter [22] and robust control [23].

Acknowledgments

This work was supported by Grant-in-Aids for Scientific Research (Grant No. 17740263, No. 17071005, and No. 15340129) and by the 21st Century COE programs on ‘‘Coherent Optical Science’’ and ‘‘Nanometer-Scale Quantum Physics’’ from the Ministry of Education, Culture, Sports, Science and Technology of Japan. M.U. acknowledges support by a CREST program of the JST.

APPENDIX A: STABILITY CONDITION WITH THE ROUTH–HURWITZ CRITERION

According to the Routh–Hurwitz criterion [21], all solutions of a polynomial equation

$$a_0\lambda^n + a_1\lambda^{n-1} + \cdots + a_{n-1}\lambda + a_n = 0 \quad (\text{A1})$$

have negative real parts if (1) all the coefficients a_i for $i = 0, 1, \dots, n$ are real and positive and (2) the determinants

$$\begin{vmatrix} a_1 & a_3 & a_5 & \cdots & a_{2i-1} \\ a_0 & a_2 & a_4 & \cdots & a_{2i-2} \\ 0 & a_1 & a_3 & \cdots & a_{2i-3} \\ 0 & a_0 & a_2 & \cdots & a_{2i-4} \\ \vdots & \vdots & \vdots & \ddots & \vdots \\ 0 & \cdots & \cdots & \cdots & a_i \end{vmatrix} \quad (\text{A2})$$

for $i = 2, 3, \dots, n$ are positive.

The system described by Eq. (22) is stable if all the eigenvalues of the 3×3 matrix on the right-hand side have negative real parts. The eigenvalue equation is given by

$$\lambda^3 + \frac{C}{\sqrt{2}\pi^{5/2}}\lambda^2 + \left(\frac{B}{\sqrt{2}\pi^{5/2}} - 1\right)\lambda + \frac{A}{\sqrt{2}\pi^{5/2}} = 0. \quad (\text{A3})$$

Applying the Routh–Hurwitz criterion to Eq. (A3), we obtain the condition for the stability given in Eq. (23).

-
- [1] L. Khaykovich, F. Schreck, G. Ferrari, T. Bourdel, J. Cubizolles, L. D. Carr, Y. Castin, and C. Salomon, *Science* **296**, 1290 (2002).
- [2] K. E. Strecker, G. B. Partridge, A. G. Truscott, and R. G. Hulet, *Nature* **417**, 150 (2002).
- [3] H. Saito and M. Ueda, *Phys. Rev. Lett.* **90**, 040403 (2003).
- [4] F. Kh. Abdullaev, J. G. Caputo, R. A. Kraenkel, and B. A. Malomed, *Phys. Rev. A* **67**, 013605 (2003).
- [5] S. Inouye, M. R. Andrews, J. Stenger, H. -J. Miesner, D. M. Stamper-Kurn, and W. Ketterle, *Nature* **392**, 151 (1998).
- [6] S. L. Cornish, N. R. Claussen, J. L. Roberts, E. A. Cornell, and C. E. Wieman, *Phys. Rev. Lett.* **85**, 1795 (2000).
- [7] For example, L. D. Landau and E. M. Lifshitz, *Mechanics*, (Pergamon, Oxford, 1960).
- [8] G. D. Montesinos, V. M. Pérez-García, and P. J. Torres, *Physica D* **191**, 193 (2004).
- [9] A. Itin, S. Watanabe, and T. Morishita, cond-mat/0506472.
- [10] G. D. Montesinos, V. M. Pérez-García, and H. Michinel, *Phys. Rev. Lett.* **92**, 133901 (2004).
- [11] M. Matuszewski, E. Infeld, B. A. Malomed, and M. Trippenbach, *Phys. Rev. Lett.* **95**, 050403 (2005); M. Trippenbach, M. Matuszewski, and B. A. Malomed, *Europhys. Lett.* **70**, 8 (2005).
- [12] H. Saito and M. Ueda, *Phys. Rev. A* **70**, 053610 (2004).
- [13] M. R. Andrews, M. -O. Mewes, N. J. van Druten, D. S. Durfee, D. M. Kurn, and W. Ketterle, *Science* **273**, 84 (1996).
- [14] B. A. Malomed, *Soliton Management in Periodic Systems*, (Springer, New York, 2006).
- [15] R. Y. Chiao, E. Garmire, and C. H. Townes, *Phys. Rev. Lett.* **13**, 479 (1964).
- [16] C. Sulem and P. L. Sulem, *The Nonlinear Schrödinger Equation*, (Springer, New York, 1999).
- [17] M. Edwards, R. J. Dodd, C. W. Clark, and K. Burnett, *J. Res. Nat. Inst. Stand. Technol.* **101**, 553 (1996).
- [18] J. M. Higbie, L. E. Sadler, S. Inouye, A. P. Chikkatur, S. R. Leslie, K. L. Moore, V. Savalli, and D. M. Stamper-Kurn, *Phys. Rev. Lett.* **95**, 050401 (2005).
- [19] J. Herbig, T. Kraemer, M. Mark, T. Weber, C. Chin, H. -C. Nägerl, R. Grimm, *Science* **301**, 1510, (2003).
- [20] V. M. Pérez-García, H. Michinel, J. I. Cirac, M. Lewenstein, and P. Zoller, *Phys. Rev. Lett.* **77**, 5320 (1996); *Phys. Rev. A* **56**, 1424 (1997).
- [21] For example, C. L. Phillips and R. D. Harbor, *Feedback Control Systems*, (Prentice Hall, New Jersey, 1988).
- [22] R. E. Kalman, *ASME J. Basic Eng.* **82**, 35 (1960).
- [23] For example, K. Zhou, J. C. Doyle, and K. Glover, *Robust and Optimal Control*, (Prentice Hall, New Jersey, 1996).